Tests of three-vector-boson nonstandard couplings

G. L. Kane, J. Vidal,* and C.- P. Yuan†
Randall Physics Laboratory, University of Michigan, Ann Arbor, Michigan 48109
(Received 23 December 1988)

We have examined the bounds on nonstandard WWV couplings that can be extracted from the existing low-energy data, without assuming some couplings are zero; we use a regularization procedure for loops that gives a gauge-invariant limit and results that do not depend on how integrations are performed. These bounds turn out to be only a little bit better than those given by unitarity requirements; in addition, some relations between parameters can be extracted. The results should be interpreted to mean that the WWZ and $WW\gamma$ vertices are not very well constrained at present, though very large deviations from standard-model values are not allowed. We have also examined how well the measurements of the W^+W^- cross section at the CERN e^+e^- collider LEP II, and WZ and $W\gamma$ production at hadron colliders, can restrict the values of the anomalous WWV couplings. We found that significant improvement, with respect to the bounds set from low-energy experiments and unitarity, can be achieved at an upgraded Fermilab Tevatron, at LEP II, and at a 400-GeV e^+e^- collider. Considerably better bounds can be set from experiments at the CERN Large Hadron Collider and at the Superconducting Super Collider.

I. INTRODUCTION

Testing the non-Abelian character of the three gauge-boson couplings of W, Z, and γ is one of the definitive checks of the SU(2)⊗U(1) gauge structure of the standard model of electroweak interactions. Until now, within experimental accuracy, all the available data agree with the predictions of the theory. No direct measurement of those WWZ and $WW\gamma$ couplings has yet been performed. High-energy machines [CERN e^+e^- collider LEP, Fermilab Tevatron, CERN Large Hadron Collider (LHC), and the Superconducting Super Collider (SSC)] will produce those vertices at the tree level, so direct measurement will be available in the future (see, for example, Refs. 1–8 for recent studies at hadron colliders and Refs. 8–13 for e^+e^- machines). Indirect measurements through radiative corrections to low-energy process[13–22] can give some bounds on the nonstandard couplings. Another possibility is to examine what kind of constraints can be extracted from unitarity.[16,22–24] The advantage of the direct production of the vertex is that no further assumptions about the behavior of the non-gauge-invariant, nonrenormalizable theory have to be made.

The WWV vertex has been extensively discussed.[25–28] Some authors[2,25] studied the behavior of the radiation zeros in $W\gamma$ scattering amplitudes[29]—predicted in the standard model—in the presence of a nongauge W magnetic moment χ_γ. Others[28] allow arbitrary "magnetic moments" χ_γ and χ_Z (the analog of the magnetic moment for the WWZ coupling) in $e^+e^-\to W^+W^-$. Effects due to magnetic moments and the electric quadrupole moment λ_γ (and the corresponding for the WWZ coupling, λ_Z) have also been studied[27] in the energy distribution of the leptons from W decay from $e^+e^-\to W^+W^-$.

In the next section of this work we describe the Lagrangian we are going to use. In Sec. III we show the bounds that can be extracted from low-energy data and then from unitarity (Sec. IV). As we will explain later the chosen procedure for the loop calculations will allow a smooth transition to the standard model when the nonstandard couplings go to zero, so the gauge invariance of the theory is restored in this limit. In Sec. V we summarize the bounds that are obtained. Sections VI and VII are devoted to the analysis of the WWV vertices at LEP II and at a 400-GeV e^+e^- collider, and at hadron colliders (Tevatron, LHC, and SSC), respectively.

Our philosophy is that we would be happy if the WWZ and $WW\gamma$ vertices were given by their gauge-theory forms, but we believe it is important to demonstrate experimentally that they are. We had initially hoped that a more complete analysis would show that they were more constrained than turned out to be the case. We also wanted to understand which future machines would be most effective in tightening the constraints. In Sec. VIII we present a discussion of the results and in Sec. IX we summarize our conclusions.

II. THE LAGRANGIAN

Several Lagrangian densities for two charged and one neutral vector boson have been proposed in past years. Neglecting the scalar component of the vector boson ($\partial_\mu V^\mu$ and $\partial_\mu W^\mu$), the most general description for the WWV interaction allows seven form factors[10,30] in this vertex. By imposing C and P symmetries separately the number of parameters can be reduced to three:

$$\mathcal{L}_{WWV}=-ie\left[(g_1^V W^\dagger_{\mu\nu}W^\mu V^\nu-W^\dagger_\mu V_\nu W^{\mu\nu})+\kappa_V W^\dagger_\mu W_\nu V^{\mu\nu}+\frac{\lambda_V}{M_W^2}W^\dagger_{\lambda\mu}W^\mu_\nu V^{\nu\lambda}\right], \tag{2.1}$$

where

$$W_{\mu\nu}=\partial_\mu W_\nu-\partial_\nu W_\mu,\quad V_{\mu\nu}=\partial_\mu V_\nu-\partial_\nu V_\mu\ . \tag{2.2}$$

W^μ is the W^- field, and V stands for either Z or γ. We do not consider the effects of ZZZ vertices (which do not occur in the gauge theory) since constraints on them are independent of constraints on W^+W^-Z vertices unless a model[7,9,31] connects them.

For $V=\gamma$, the first term of (2.1), with $g_1^V=1$, corresponds to the covariant derivative prescription for spin-1 charged particles. The second (κ_V) and the third (λ_V) are related to the magnetic dipole and electric quadrupole moments by

$$\mu_W=\frac{e}{2M_W}(1+\kappa_V+\lambda_V)\ , \tag{2.3}$$

$$Q_W=-\frac{e}{M_W^2}(\kappa_V-\lambda_V)\ . \tag{2.4}$$

Using these, the Lagrangian (2.1) coincides with the WWV sector of the one proposed by Grifols, Peris, and Solá.[14,15] It is a generalization of the electromagnetic interaction of spin-1 charged particles[32] to include the weak interaction of the Z boson ($\lambda_V=-\lambda_j$ and $\kappa=\chi$ have been defined in order to follow the notation of Ref. 14):

$$\mathcal{L}=-\tfrac{1}{2}\hat{G}^\dagger_{\mu\nu}\hat{G}^{\mu\nu}+M_W^2W_\mu^\dagger W^\mu+\tfrac{1}{2}M_Z^2Z^\mu Z_\mu -\tfrac{1}{4}\sum_{j=\gamma,Z}\hat{F}^{\mu\nu}_j\hat{F}_{j\mu\nu}+\sum_{j=\gamma,Z}\frac{ig_j\lambda_j}{M_W^2}\hat{F}^{j}_{\mu\nu}\hat{G}^{\dagger\mu\rho}\hat{G}^{\nu}_{\rho}\ , \tag{2.5}$$

with

$$\begin{aligned}\hat{G}_{\mu\nu}&\equiv(\partial_\mu-ig_\gamma A_\mu-ig_Z Z_\mu)W_\nu -(\partial_\nu-ig_\gamma A_\nu-ig_Z Z_\nu)W_\mu\ ,\\ \hat{F}^{j}_{\mu\nu}&\equiv F^j_{\mu\nu}+ig_j\chi_j(W_\mu^\dagger W_\nu-W_\nu^\dagger W_\mu)\ ,\end{aligned} \tag{2.6}$$

and

$$\begin{aligned}&F^\gamma_{\mu\nu}=\partial_\mu A_\nu-\partial_\nu A_\mu,\quad F^Z_{\mu\nu}=\partial_\mu Z_\nu-\partial_\nu Z_\mu\ ,\\ &g_\gamma=g\sin\theta_W=e,\quad g_Z=g\cos\theta_W\ .\end{aligned} \tag{2.7}$$

Values of λ_j and $\Delta\chi_j$ ($\equiv\chi_j-1$) differing from 0 will indicate deviations from the standard model. As we will show later, it is convenient for our purpose to adopt this parametrization because it allows us to separate the standard-model amplitudes from the nonstandard ones.

III. LOW-ENERGY PROCESSES

No processes have been observed experimentally in which the W^+W^-Z or $W^+W^-\gamma$ vertices occur at the tree level, because present colliders do not have sufficient energy or luminosity. However, these vertices occur in loops, and contribute to observed processes. Although loop contributions are small, if the deviation from the standard-model predictions were very large, an effect might have been observed. As discussed in the Introduction, a number of authors have already examined what bounds could be extracted from the low-energy data, but generally they have made assumptions that some parameters were very small or fixed in order to get good limits on others. We have avoided such assumptions.

If the WWV vertices deviate from their standard-model values, the resulting theory is necessarily not gauge invariant and there is no unique answer to any loop calculation. That does not mean one should not study such possibilities, since nature could behave that way; deviations would imply that the low-energy theory was an effective one, and a more basic theory would hold at a scale characterized by some parameter Λ with dimensions of mass.

A particular concern that arises in such a situation is that there will exist Lagrangians, gauges, or regularization procedures where apparent constraints of the form $\Lambda^4\delta<\Delta$ exist (as they have for some authors), where δ is one of our parameters and Δ is an experimental error or limit, while normally the constraints are of the form $\Lambda^2\delta<\Delta$. From our Lagrangian and regularization procedures none of the $\Lambda^4\delta$ constraints occur, which means that none of our constraints is unduly strong or likely to change because of the regularization, etc. Our goal is to determine what kind of information on the nonstandard parameters we can extract from the existing low-energy experimental data. Because in our calculation some one-loop diagrams with ultraviolet divergences are involved, we have to fix a procedure to obtain finite results. In the standard model the divergences appearing in loop calculations can be removed by an adequate renormalization of some of the parameters, and Ref. 33 shows how to get finite results for physical quantities beyond the tree approximation by fixing three free parameters in low-energy experiments. As was already pointed in Ref. 14, the new interaction present in the Lagrangian (2.5) has to be taken into account in the redefinitions of the electroweak parameters. We will use a regulator only for the ultraviolet-divergent loop integrals that involve the new nonstandard couplings. The advantage of this procedure is that we do not break the gauge invariance of the standard-model part; there is a smooth transition to the standard model when the new couplings go to zero. For the nonstandard part we will only keep terms in positive powers of the new scale, Λ, and neglect logarithmic terms. It is important to understand that we are not giving a general analysis of this entire problem, but an approximate one which is appropriate for the level of accuracy we need and consistent with the conclusions we find. In particular, one-loop radiative corrections to the normal standard model are numerically smaller than the deviations we are sensitive to, so we can neglect them.

As it is well known the use of a regulator has the advantage, over the momentum-cutoff regularization scheme, that the results are always well defined and they do not depend on the procedures used in performing the integrations. Only three types of ultraviolet-divergent integrals are involved in our one-loop calculation, when neglecting the logarithmic divergent terms:

$$I_1=\int\frac{d^4p}{(2\pi)^4}\frac{\{p^2,p^3,p^4\}}{[p^2-M_1^2][(p+q)^2-M_2^2]}\ ,$$
$$I_2=\int\frac{d^4p}{(2\pi)^4}\frac{\{p^2\}}{[(p+q)^2-M_1^2][(p+q+k)^2-M_2^2]}\ , \quad (3.1)$$
$$I_3=\int\frac{d^4p}{(2\pi)^4}\frac{\{1,p^2\}}{p^2-M_1^2}\ ,$$

with $M_{1,2}$ the masses of the gauge bosons W, Z, or γ. The first and second integrals come from the three-point-vertex (WWV) contribution to the W and Z self-energies and fermion-fermion-V vertex (when the fermion mass is neglected), respectively, and the third one takes into account the four-point vertex ($WWWW$ or $WWVV$) contribution to the W and Z self-energies. We consistently regularize these integrals with the minimum number of regulators that makes all of them finite. Then our integrals become

$$I_1^R=\int\frac{d^4p}{(2\pi)^4}\left[\frac{\Lambda^2}{p^2-\Lambda^2}\right]^2\left[\frac{\Lambda^2}{(p+q)^2-\Lambda^2}\right]^2\times\frac{\{p^2,p^3,p^4\}}{(p^2-M_1^2)[(p+q)^2-M_2^2]}\ ,$$
$$I_2^R=\int\frac{d^4p}{(2\pi)^4}\left[\frac{\Lambda^2}{(p+q)^2-\Lambda^2}\right]^2\left[\frac{\Lambda^2}{(p+q+k)^2-\Lambda^2}\right]^2\times\frac{\{p^2\}}{[(p+q)^2-M_1^2][(p+q+k)^2-M_2^2]}\ , \quad (3.2)$$
$$I_3^R=\int\frac{d^4p}{(2\pi)^4}\left[\frac{\Lambda^2}{p^2-\Lambda^2}\right]^4\frac{\{1,p^2\}}{p^2-M_1^2}\ ,$$

where Λ is the scale where the new physics shows up. Our underlying attitude is that if the gauge theory is to fail, then effectively all the particles are composites, and we are trying to guess a sensible procedure to represent how integrals becomes convergent from structure effects.

Three low-energy processes—μ decay, $e\mu$ Coulomb scattering, and the ratio of $\nu_\mu e$ and $\bar{\nu}_\mu e$ scattering—can be used to fix three electroweak parameters[33] of the theory: G_F, α, and $\sin^2\theta_W$ ($\equiv s_W^2$),

$$\frac{G_F}{\sqrt{2}}=\frac{g^2}{8M_W^2},\quad \alpha=\frac{g^2s_W^2}{4\pi},\quad \tfrac{1}{4}(1-\xi)=s_W^2\ , \quad (3.3)$$

where $\xi=v/a$ is the ratio of the vector and axial-vector couplings of the electron current to the gauge boson Z.

Because we are interested in seeing how the new interactions affect the redefinitions of these three free parameters, we write the nonstandard contributions at one-loop level[14,33] in the form

$$\frac{G_F}{\sqrt{2}}=\frac{g^{(1)2}}{8M_W^{(1)2}}(1+\delta_1),\quad \alpha=\frac{g^{(1)2}s_W^{(1)2}}{4\pi}(1+\delta_2)$$
$$\tfrac{1}{4}(1-\xi)=s_W^{(1)2}(1-\delta_3)\ . \quad (3.4)$$

Then

$$s_W^{(1)2}=\tfrac{1}{4}(1-\xi)(1+\delta_3)\equiv s_W^2(1+\delta_3)\ ,$$
$$g^{(1)2}=\frac{16\pi\alpha}{(1-\xi)}(1-\delta_2-\delta_3)\equiv g^2(1-\delta_2-\delta_3)\ ,$$
$$M_W^{(1)2}=\frac{2\sqrt{2}\pi\alpha}{(1-\xi)G_F}(1+\delta_1-\delta_2-\delta_3)\equiv M_W^2(1+\delta_1-\delta_2-\delta_3)\ , \quad (3.5)$$
$$M_Z^{(1)2}=\frac{2\sqrt{2}\pi\alpha}{(1-\xi)[1-\frac{1}{4}(1-\xi)]G_F}\times\left[1+\delta_1-\delta_2-\delta_3+\frac{s_W^2}{c_W^2}\delta_3\right]\equiv M_Z^2\left[1+\delta_1-\delta_2-\delta_3+\frac{s_W^2}{c_W^2}\delta_3\right]\ ,$$

where $C_W^2=1-S_W^2$. These are the bare quantities we have to use to get the expressions for the observables at one loop. The $\delta_{1,2,3}$ are the contributions of the new interaction vertices to the different amplitudes involved in the processes named above. An explicit calculation gives the following expression for these shifts, in terms of the new-physics scale Λ:

$$\delta_1=-\frac{g^2}{32\pi^2}\frac{\Lambda^2}{M_W^2}[\Delta\chi_Z+(c_W^2+\tfrac{1}{2})\Delta\chi_Z^2+\Delta\chi_\gamma^2s_W^2]\ ,$$
$$\delta_2=\frac{g^2}{24\pi^2}\frac{\Lambda^2}{M_W^2}s_W^2(3\lambda_\gamma+\Delta\chi_\gamma\lambda_\gamma+\tfrac{1}{2}\Delta\chi_\gamma^2-\lambda_\gamma^2)+\frac{g^2}{32\pi^2}\frac{1}{3}\frac{\Lambda^4}{M_W^4}s_W^2\lambda_\gamma^2\ , \quad (3.6)$$
$$\delta_3=\frac{g^2}{32\pi^2}\frac{1}{3}\frac{\Lambda^2}{M_W^2}\{c_W^2[6(\lambda_Z+\lambda_\gamma)+2(\Delta\chi_Z\lambda_\gamma+\Delta\chi_\gamma\lambda_Z)+2\Delta\chi_Z\Delta\chi_\gamma-4\lambda_\gamma\lambda_Z]-\tfrac{1}{2}\Delta\chi_\gamma\}+\frac{g^2}{32\pi^2}\frac{1}{3}\frac{\Lambda^4}{M_W^4}c_W^2\lambda_Z\lambda_\gamma\ .$$

The results, in the limit of small couplings (i.e., second order in couplings $\to 0$), only differ by a factor of $\frac{1}{3}$ from the ones given in Ref. 14. As we checked, the absence of a Λ^4 term in δ_1 is due to an exact cancellation among the various diagrams contributing to the W-boson self-energy at zero momentum [$\Pi_W(0)$].

In the following, we are going to examine several existing low-energy experiments, and extract the constraint equations on the four form factors we introduced in the Lagrangian (2.5).

A. Neutrino-nucleon scattering

The $\rho_{\nu N}$ parameter is defined through the ratio of neutral and charged currents in νN scattering as

$$R_{\nu N}\equiv\frac{\sigma(\nu N\to\nu X)}{\sigma(\nu N\to\mu X)}=\rho_{\nu N}^2(\tfrac{1}{2}-s_W^2+\tfrac{20}{27}s_W^4)\ , \quad (3.7)$$

where the ratio of antiquark momentum to quark momentum distributions in the nucleon has been neglected for simplicity. The computation of the nonstandard

contributions to $R_{\nu N}$ up to one loop can be easily done by using the scheme shown in the previous section, and introducing the appropriate regulator (3.2) to perform the ultraviolet-divergent integrations. The result can be written as

$$R_{\nu N}=(1-\delta_1)^2(\tfrac{1}{2}-s_W^2+\tfrac{20}{27}s_W^4)\ . \tag{3.8}$$

One can now interpret δ_1 as the contribution of the new interaction described by the Lagrangian (2.5) to the $\rho_{\nu N}$ parameter, and then use the accuracy of the experimental measurement to set a bound on the deviations of these two form factors, $\Delta\chi_Z$ and $\Delta\chi_\gamma$, from the standard-model predictions ($\Delta\chi_Z=\Delta\chi_\gamma=0$). A two-parameter ($\sin\theta_W$ and $\rho_{\nu N}$) fit[34] to the data on deep-inelastic scattering determines the value of $\rho_{\nu N}$ within an accuracy $\Delta\rho_{\nu N}=\pm 0.015$, so we can write

$$|\delta_1|\leq 0.015\ . \tag{3.9}$$

For $\Lambda=1$ TeV, the resulting bounds on $\Delta\chi_Z$ and $\Delta\chi_\gamma$ are shown in Fig. 1. The allowed values of the parameters are in the region between dashed lines, and the mean values lie on the solid line. Notice that because the proximity of the bounds, one can take $\Delta\chi_\gamma$ and $\Delta\chi_Z$ to be related through the equation

$$\frac{[\Delta\chi_Z+1/(2c_W^2+1)]^2}{[1/(2c_W^2+1]^2}+\frac{\Delta\chi_\gamma^2}{[1/(2s_W\sqrt{C_W^2+1/2})]^2}=1\ , \tag{3.10}$$

which is the average curve in Fig. 1. As can be seen, (3.10) is a scale-independent relation and for bigger Λ it becomes more accurate to describe the allowed region of parameters. If the value $\Delta\rho_{\nu N}=\pm 0.015$ is thought to be too optimistic, the dashed lines get separated somewhat more, but the parameters $\Delta\chi_Z,\Delta\chi_\gamma$ still approximately lie on the ellipse. In Ref. 14, the bound $\Delta\chi_Z\leq 0.013$ (for $\Lambda=1$ TeV) can be now reproduced by Fig. 1 (for $\Delta\chi_\gamma=0$)

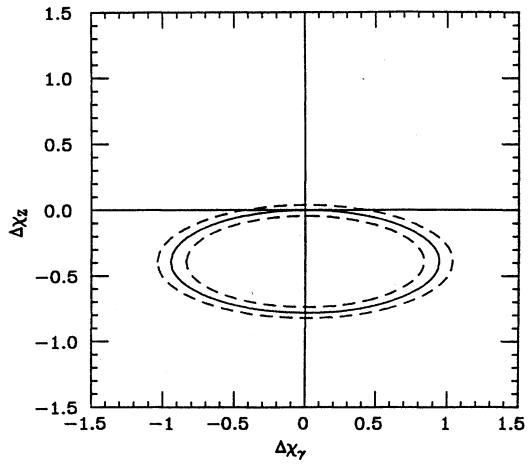

FIG. 1. Values of $\Delta\chi_Z$ and $\Delta\chi_\gamma$ (region enclosed by dashed lines) allowed by the measurement of the ρ parameter in νN experiments. A value of the new physics scale $\Lambda=1$ TeV has been used. The solid line is the average curve.

apart from a factor of 3 due to the regularization procedure we adopted.

We also checked the process[18] $(\bar{\nu})_\mu e\to(\bar{\nu})_\mu e$. As can be easily seen from its amplitude,[14] the deviation from the standard cross section, at low energy, is proportional to δ_1. Because of the errors in the experimental measurements,[34] one finds that the bound on δ_1 is almost 20 times looser than the one given by (3.9), so the constraint on δ_1 coming from the $\rho_{\nu N}$ parameter is the best we can get so far.

B. Polarized electron-deuterium asymmetry

We have calculated the nonstandard one-loop correction to the polarized electron-deuterium asymmetry in order to set bounds on the new parameters. The corrections to all the relevant vertices and self-energies have been computed up to one loop. The results for the gauge boson self-energies are given in Sec. 1 of Appendix A. The deviations induced by the new couplings in the a_1, a_2 parameters defined though[35]

$$\frac{A^{eD}(x,y)}{q^2}=\frac{-9G}{5\sqrt{2}\pi\alpha}\left[a_1+a_2\frac{1-(1-y)^2}{1+(1-y)^2}\right]\ , \tag{3.11}$$

are given by

$$\begin{aligned}a_1(1+\Delta a_1)&=(\tfrac{5}{9}s_W^2-\tfrac{1}{4})(1-\delta_1)\ ,\\ a_2(1+\Delta a_2)&=(s_W^2-\tfrac{1}{4})(1-\delta_1)\ .\end{aligned} \tag{3.12}$$

Now the results of Ref. 21, where only the anomalous $WW\gamma$ coupling was considered, can be obtained as a special case of our formula [a factor $\frac{1}{3}$, due again to the regularization scheme, appears in (3.12)] just by putting all the nonstandard couplings of the Z boson equal to zero. For $\Lambda\sim 1$ TeV, because the momentum transfer q^2 is (in average) 1.6 GeV^2, the contributions of quartic terms in Λ, $(q^2/M_W^2)(\Lambda^4/M_W^4)$, turn out to be 30 times smaller than the quadratic terms (δ_1). Therefore we can only get a bound again on δ_1. The experimental measured values[36] give

$$\begin{aligned}\delta_1\simeq\Delta a_1&\leq\frac{|\text{Abs. error }(a_1)|}{a_1}=0.27\ ,\\ \delta_1\simeq\Delta a_2&\leq\frac{|\text{Abs. error }(a_2)|}{a_2}=1.6\end{aligned} \tag{3.13}$$

If $\Lambda\sim 1$ TeV, the bound we have on δ_1 is looser than the one obtained in Eq. (3.9) from the $\rho_{\nu N}$ parameter measurement. Again, the bound would be tighter for a bigger new-physics scale Λ.

C. $e^+e^-\to\mu^+\mu^-$. Cross section and forward-backward asymmetry

Data on muon-pair production in e^+e^- experiments can also provide some information about the allowed values of the new couplings. The V-V and A-A parts of the amplitude for this process can be expressed in the form

$$T_{VV}=-\frac{e^2}{S}\bar{v}(e)\gamma^{\nu}u(e)\bar{u}(\mu)\gamma_{\nu}v(\mu)(1+h_{VV}) ,$$
$$T_{AA}=-\frac{e^2}{S}\bar{v}(e)\gamma^{\nu}\gamma_5 u(e)\bar{u}(\mu)\gamma_{\nu}\gamma_5 v(\mu)h_{AA} , \tag{3.14}$$

with $S=E^2_{\text{c.m}}$, and

$$h_{VV,AA}=h^{\text{SM}}_{VV,AA}+\Delta h_{VV,AA} . \tag{3.15}$$

In Eq. (3.14), $h_{VV,AA}$ are the effective couplings. In Eq. (3.15) we have separated the standard contributions $h^{\text{SM}}_{VV,AA}$ from the nonstandard ones $\Delta h_{VV,AA}$. The expression for Δh_{AA} (Δh_{VV}), which includes one-loop nonstandard corrections, is given in Sec. 2 of Appendix A. Keeping only leading terms in Λ and using the formulas in Sec. 1 of Appendix A for the gauge-bosons self-energies, the expressions become

$$h_{VV,AA}=h^{\text{SM}}_{VV,AA}\left[1+\frac{S}{S-M_Z^2}\delta\right] , \tag{3.16}$$

where

$$\delta=\frac{g^2}{32\pi^2}\frac{1}{3}\frac{\Lambda^4}{M_W^4}[c_W^2\lambda_Z^2+(s_W^2-c_W^2)\lambda_Z\lambda_\gamma-s_W^2\lambda_\gamma^2] . \tag{3.17}$$

The standard couplings $h^{\text{SM}}_{VV,AA}$ are given by

$$h^{\text{SM}}_{VV}\equiv\frac{S}{S-M_Z^2}\frac{1}{16s_W^2c_W^2}v^2 ,$$
$$h^{\text{SM}}_{AA}\equiv\frac{S}{S-M_Z^2}\frac{1}{16s_W^2c_W^2}a^2 , \tag{3.18}$$

with

$$v=(-1+4s_W^2),\quad a=-1 . \tag{3.19}$$

Then the nonstandard contributions to the cross section

$$R_{\mu\mu}\equiv\frac{\sigma(e^+e^-\to\mu^+\mu^-)}{\sigma_{\text{QED}}}=1+2h_{VV}+(h_{VV}+h_{AA})^2 , \tag{3.20}$$

and forward-backward asymmetry

$$A_{FB}=\frac{3}{4R_{\mu\mu}}(2h_{AA}+4h_{AA}h_{VV}) , \tag{3.21}$$

can be written as

$$\Delta R_{\mu\mu}=2\frac{S}{S-M_Z^2}[(h^{\text{SM}}_{VV}+h^{\text{SM}}_{AA})^2+h^{\text{SM}}_{VV}]\delta , \tag{3.22}$$

and

$$\Delta A_{FB}=\frac{3}{2R_{\mu\mu}}\frac{S}{S-M_Z^2}(h^{\text{SM}}_{AA}+4h^{\text{SM}}_{AA}h^{\text{SM}}_{VV})\delta , \tag{3.23}$$

respectively.

For low-energy experiments, where nonleading terms q^4/M_W^4 are neglected, the Λ^4 terms do not contribute. As can be checked from the expressions in in Sec. 2 of Appendix A, the nonstandard deviation for the observables is then strongly suppressed by the factor q^2/M_W^2, so no good bound on the parameters can be set. This result also holds for the energies of the DESY and SLAC e^+e^- storage rings PETRA and PEP.

For higher energies (≥ 30 GeV), assuming Λ^4 terms dominate (in fact the quartic terms in Λ turn out to be ~ 20 times bigger than the corresponding quadratic ones for $\Lambda=1$ TeV and $\sqrt{S}\geq 30$ GeV), the expressions of ΔR and ΔA_{FB} shown above can be safely used. Assuming[34] $\Delta R_{\mu\mu}\sim 0.02$ and $\Delta A_{FB}/A_{FB}\sim 30\%$ (results from PETRA and PEP data), and due to the factor $S/(S-M_Z^2)$ present in Eqs. (3.22) and (3.23), and the effective couplings $h^{\text{SM}}_{VV,AA}$, we conclude that the combination of parameters δ cannot be constrained better than

$$|\delta|\leq 1.5 . \tag{3.24}$$

(Bigger values of the new-physics scale Λ would improve this bound, but we will consistently restrict ourselves to $\Lambda\sim 1$ TeV.)

As we will show later, this loose bound can be substantially improved by measuring the mass shift of the Z, where the nonstandard couplings enter in the same combination as (3.17).

D. Mass shift of the gauge bosons

The physical masses of the gauge bosons are defined as the poles of the vector boson full propagators. Up to one loop, only considering nonstandard contributions, the physical masses are given by

$$(M^2_{W,Z})_{\text{ph}}=M^{(1)2}_{W,Z}-\Pi_{W,Z}(M^2_{W,Z}) , \tag{3.25}$$

where the self-energies, Π_W and Π_Z, are given in Appendix A. From Eq. (3.5), one gets the final expressions of the mass shift due to the new interaction terms as

$$\Delta M_W^2=M_W^2(\delta_1-\delta_2-\delta_3)+\Pi_W(M_W^2) ,$$
$$\Delta M_Z^2=M_Z^2\left[\delta_1-\delta_2-\delta_3+\frac{s_W^2}{c_W^2}\delta_3\right]+\Pi_Z(M_Z^2) . \tag{3.26}$$

The shift of the ρ_M parameter ($\Delta\rho_M=\Delta M_W^2/M_W^2-\Delta M_Z^2/M_Z^2$) is then derived from the previous equations. Notice that δ_1 and δ_2 contributions cancel out, so that

$$\Delta\rho_M=\frac{\Pi_W(M_W^2)}{M_W^2}-\frac{\Pi_Z(M_Z^2)}{M_Z^2}-\frac{s_W^2}{c_W^2}\delta_3 . \tag{3.27}$$

The complete expression for the shifts can be obtained from the formulas shown in Appendix A, but we will only keep the leading term in Λ (for $\Lambda\geq 1$ TeV). In this approximation the $\Delta\rho_M$ and ΔM_Z^2 are given by

$$\Delta\rho_M\simeq\frac{g^2}{32\pi^2}\frac{1}{3}\frac{\Lambda^4}{M_W^4}s_W^2(\lambda_\gamma^2-\lambda_Z\lambda_\gamma) ,$$
$$\frac{\Delta M_Z^2}{M_Z^2}=\frac{g^2}{32\pi^2}\frac{1}{3}\frac{\Lambda^4}{M_W^4}[c_W^2\lambda_Z^2+(s_W^2-c_W^2)\lambda_Z\lambda_\gamma-s_W^2\lambda_\gamma^2] . \tag{3.28}$$

Using now the experimental uncertainties[34] $|\Delta\rho_M|\leq 3\%$ and $|\Delta M_Z|/M_Z\leq 2\%$, we are able to restrict the values

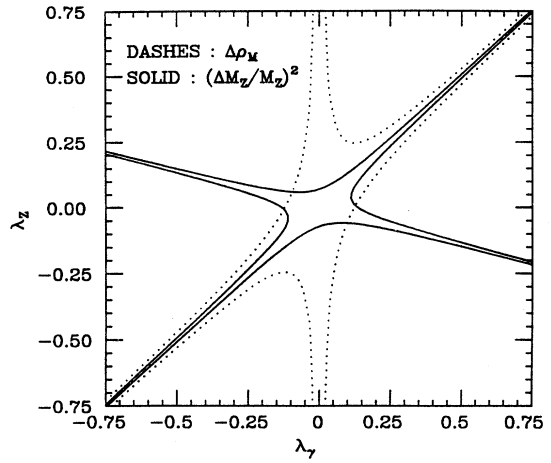

FIG. 2. Values of λ_Z and λ_γ allowed by the measurement of the ρ_M parameter (region enclosed by dotted lines) and the mass of the Z (solid). A value of $\Lambda=1$ TeV has been used.

of the quadrupole terms $\lambda_{Z,\gamma}$ to the ones enclosed by the solid (bounds from ΔM_Z) and dotted (bounds from $\Delta\rho_M$) lines shown in Fig. 2, for a value of $\Lambda=1$ TeV. The region enclosed by both the solid and dashed lines is the allowed region for λ_Z and λ_γ. We see that we can impose the approximate relation

$$\lambda_\gamma=\lambda_Z \ , \tag{3.29}$$

for $|\lambda_{\gamma,Z}|\geq 0.1$. Recall that this numerical value is found by setting $\Lambda=1$ TeV, and also keeping only Λ^4 terms. We have also calculated the contributions from Λ^2 terms and verified that it is safe to impose the constraint

$$\lambda_\gamma=\lambda_Z \quad \text{for } |\lambda_{\gamma,Z}|>0.15 \ , \tag{3.29'}$$

for $\Lambda=1$ TeV. For a bigger Λ the bounds will be more restrictive than the ones in Fig. 2. The result qualitatively agrees with the one in Ref. 15, which was obtained by taking both $\Delta\chi_i=0$ (which we have not assumed).

IV. UNITARITY

From the analyses shown in the previous sections, one can see that some useful constraints can be set on the magnetic-moment parameters $\Delta\chi_i$, basically from neutrino-nucleon scattering [Eq. (3.9) and Fig. 1]. Regarding the λ_i parameters, the mass shift of the gauge bosons [Eqs. (3.28) and Fig. 2] restricts the allowed values to be in a well-defined region of the λ_γ-λ_Z plane, but no bound on the absolute magnitude of either λ_Z or λ_γ can be extracted from the measurement. The situation will be improved by fixing an upper bound to the absolute value of the λ_Z parameter, coming from unitarity conditions.

The authors of Ref. 23 found that by imposing unitarity on the amplitude of the elastic process $f_1\bar{f}_2\to f_3\bar{f}_4$ for a certain combination of leptons in the initial state, the following condition on the nonstandard amplitude for W^+W^- production through the Z exchange could be established

$$\left[\sum_{\lambda_2\lambda_3}|A^Z_{\lambda_2\lambda_3}|^2\right]^{1/2}\leq\frac{1}{\alpha\beta^{3/2}}\sqrt{\tfrac{3}{10}}4s_W^2\left[1-\frac{M_Z^2}{S}\right] , \tag{4.1}$$

where $\beta=[1-(4M_W^2/S)]^{1/2}$, and λ_2,λ_3 define the polarization state of gauge bosons. In our notation (2.5) the different nonstandard amplitudes contributing to (4.1) can be written as

$$\begin{aligned} A^Z_{\pm 0}&=A^Z_{0\pm}=\gamma(\Delta\chi_Z-\lambda_Z) \ , \\ A^Z_{\pm\pm}&=-\frac{S}{2M_W^2}\lambda_Z \ , \\ A^Z_{00}&=\gamma^2 2\Delta\chi_Z \ , \end{aligned} \tag{4.2}$$

where the factor γ is $\gamma=E_W/M_W$.

At the energy scale $\sqrt{S}=\Lambda$ (assuming that the couplings have no energy dependence for $S<\Lambda^2$ and drop to zero at Λ), only the amplitudes $A^Z_{\pm\pm}$ and A^Z_{00} are relevant, and the condition (4.1) takes the form

$$2\lambda_Z^2+(\Delta\chi_Z)^2\leq\frac{M_W^4}{\Lambda^4}\frac{96}{5}\frac{s_W^2}{\alpha^2} \ . \tag{4.3}$$

If, as we did in the previous sections, one fixes the new-physics scale Λ to be 1 TeV, then the absolute bound on the quadrupole moment that we can extract is

$$|\lambda_Z|\leq 0.6 \ . \tag{4.4}$$

Combining with the bounds obtained from the mass shifts (Fig. 2), we conclude that λ_γ also has to be smaller than 0.6 and therefore no value bigger than 0.6 for quadrupole moment $|\lambda_i|$ is allowed. Other bounds on λ_γ can be obtained, for instance, from the $(g-2)$ factor of the muon,[19,20] but the value they[20] found is at least 1 order of magnitude bigger than the one given above.

V. SUMMARY OF BOUNDS FROM DATA

From Secs. III and IV, the bounds on the four form factors (2.5), from the existing low-energy data, can be summarized as follows.

(i) The bounds on these four parameters, $\Delta\chi_\gamma$, $\Delta\chi_Z$, λ_γ, and λ_Z, can be found from Figs. 1 and 2 and Eq. (4.4).

(ii) We can now derive from (i) the lower and upper bounds on each single parameter as

$$\begin{aligned} &-0.6\leq\lambda_\gamma\leq 0.6, \quad -0.6\leq\lambda_Z\leq 0.6 \ , \\ &-0.94\leq\Delta\chi_\gamma\leq 0.94, \quad -0.80<\Delta\chi_Z\leq 0 \ , \end{aligned} \tag{5.1}$$

where for $\Delta\chi_Z,\Delta\chi_\gamma$ we used the average curve in Fig. 1. From there, the uncertainty of $\Delta\chi_Z$ is about ± 0.04, for $\Lambda=1$ TeV.

(iii) To simplify the discussion in the next sections we will take the following approximations: (a) Use (3.10) as the relation between $\Delta\chi_\gamma$ and $\Delta\chi_Z$, whenever both of them are present, to reduce the number of free parameters to three. (b) Set $\lambda_\gamma=\lambda_Z$, for $|\lambda_\gamma|\geq 0.15$ to give two parameters. Otherwise, treat λ_γ and λ_Z as two independent parameters.

Comparing these results with the ones given by impos-

ing unitarity,[23] for $\Lambda=1$ TeV,

$$|\lambda_\gamma|\leq 1.0,\quad |\lambda_Z|\leq 0.6\ ,$$
$$|\Delta\chi_Z|\leq 0.85,\quad |\Delta\chi_\gamma|\leq 1.86\ , \tag{5.2}$$

one can see that the bounds on the magnitude of the parameters are of the same order (a factor of 2 for $\Delta\chi_\gamma$) as the ones we extracted from low-energy data. The main impact of existing data is to effectively reduce the number of free parameters from four to two, approximately.

VI. W-PAIR PRODUCTION IN e^+e^- COLLISIONS

We have shown how well the low-energy data can constrain the nonstandard parameters of the Lagrangian (2.5). What we want to address now is a twofold question: (1) What kind of constraints on the new parameters could be obtained from $e^+e^-\to W^+W^-$, at LEP and ILC energies, assuming the measurements agree with the prediction of the standard model within the experimental uncertainties? (ILC is an e^+e^- collider with $\sqrt{S}$ above about 400 GeV, and luminosity above about 10^{32} $\text{cm}^{-2}\,\text{sec}^{-1}$. Its possible parameters and physics were studied extensively at Snowmass, 1988, in Ref. 8.) (2) What is the maximum allowed deviation of the cross section from the standard model, imposing the constraints obtained from low-energy experiments discussed in the previous section? Related questions have been studied by a number of authors,[10,11] but our perspective is a little different because of our analysis of the low-energy data, and because we do not assume any of the parameters are determined by theoretical arguments.

In order to show as much as possible the dependence of the observables on those four form factors, we study the cross section for different polarized final states. The helicity amplitudes are given in Refs. 3 and 37, where the relevant form factors f_1^V, f_2^V, and f_3^V are

$$f_1^V=1-\frac{S}{2M_W^2}\lambda_V,\quad f_2^V=-\lambda_V,\quad f_3^V=2+\Delta\chi_V-\lambda_V\ . \tag{6.1}$$

The computation of the cross section can now be carried out and it shows that, for the longitudinal-W cross section (σ_{LL}), the deviation from the standard model only depends on the magnetic moments $\Delta\chi_\gamma$ and $\Delta\chi_Z$. For transverse W's (σ_{TT}), only the quadrupole moments λ_γ and λ_Z give nonstandard contributions. For the longitudinal-transverse cross section ($\sigma_{LT}=\sigma_{TL}$), and of course σ_{tot}, both sets of parameters contribute to the deviations.

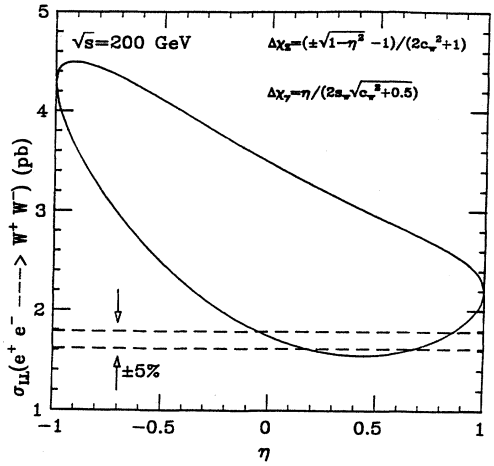

FIG. 3. Cross section for longitudinal W's (solid), at LEP II, as a function of $\Delta\chi_Z$ and $\Delta\chi_\gamma$. Existing low-energy data require that results must lie on the solid curve. Values of the anomalous couplings, allowing for the measurement of the cross section with a 5% accuracy, are the regions of the solid line enclosed by dashed lines. Note that if an accuracy of order 10% is the best that can be done (for σ_{LL}, not for σ_{tot}), then this measurement only fixes $-0.15\leq\eta\leq 0.90$ with values of $\Delta\chi_i$ determined by the equations shown.

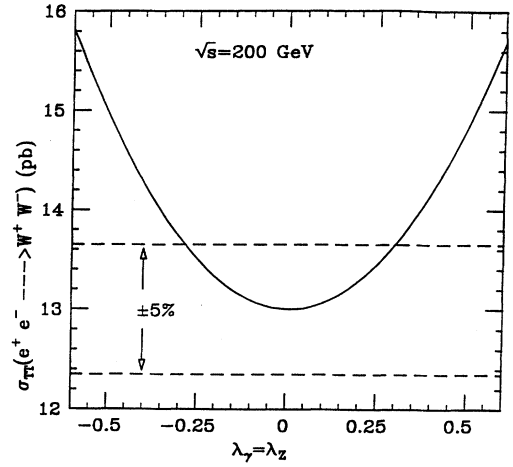

FIG. 4. Cross section for transverse W's (solid), at LEP II as a function of λ_Z ($=\lambda_\gamma$). Values of the anomalous couplings, assuming measurement of the cross section with a 5% accuracy, are the regions of the solid line enclosed by the dashed lines.

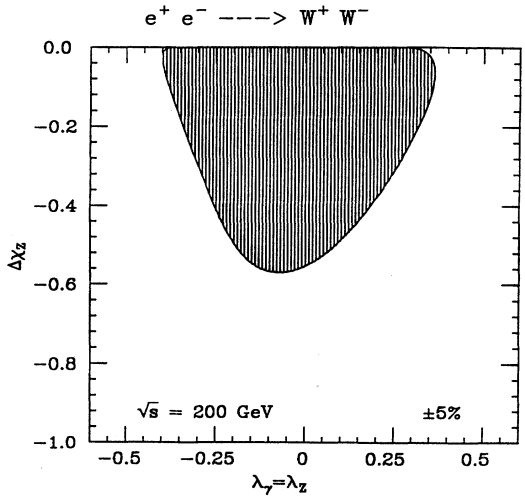

FIG. 5. Bounds on $\Delta\chi_Z$ and λ_Z ($=\lambda_\gamma$) from the measurement of the total cross section $\sigma(e^+e^-\to W^+W^-)$ at LEP II ($\sqrt{S}=200$ GeV). The shaded area is the region of the parameters that give a cross section in agreement with the standard model within a 5% accuracy.

In order to evaluate these deviations, we fix the energy for LEP II at $\sqrt{S}=200$ GeV. We will use the approximate bounds summarized in Sec. V to do the following analysis.

The behavior of σ_{LL} can be seen in Fig. 3 in terms of the free variable η ($-1\leq\eta\leq 1$), defined by (because of the constraint of Fig. 1)

$$\Delta\chi_\gamma=\frac{1}{2[s_W^2(c_W^2+1/2)]^{1/2}}\eta\ ,$$
$$\Delta\chi_Z=\frac{1}{2(c_W^2+1/2)}(\pm\sqrt{1-\eta^2}-1)\ . \tag{6.2}$$

In σ_{LL} the nonstandard contribution $\Delta\sigma_{LL}$ can be as big as 3 pb ($\sim 2\sigma_{LL}^{\rm SM}$). Therefore, if σ_{LL} is shown to be in agreement with the standard-model prediction up to 5%, one can set a better bound on $\Delta\chi_\gamma$ and $\Delta\chi_Z$ (as shown in Fig. 3) than the one set by measuring the total cross section $\sigma_{\rm tot}$ at the same accuracy (Figs. 5 and 6 below).

Notice that there are two allowed regions in Fig. 3. The one nearby $\eta=0.8$ is due to some cancellations between these two parameters $\Delta\chi_Z$ and $\Delta\chi_\gamma$. If one simply puts $\Delta\chi_Z$ or $\Delta\chi_\gamma$ to zero (as some authors do) in order to set bounds on $\Delta\chi_\gamma$ or $\Delta\chi_Z$, one will never find the allowed region far from $\eta=0$ in Fig. 3. Note also that if σ_{LL} (which is a small part of the total WW cross section) can only be measured to accuracies of order 10% or worse, then the entire region $-0.15\leq\eta\leq 0.90$ will be allowed.

The σ_{TT} is given in Fig. 4 (assuming $\lambda_Z=\lambda_\gamma$ in the whole allowed region). In this case the maximum deviation is reached for extreme values of λ, and $\Delta\sigma_{TT}$ can be as big as $\sigma_{TT}^{\rm SM}$. If one can measure the cross section σ_{TT} and find it agrees with the standard-model prediction up to 5%, then one can get a better bound on both $|\lambda_Z|$ and $|\lambda_\gamma|$ (≤ 0.2) than the ones obtained from the total cross section at the same accuracy (6.3).

For σ_{LT} and $\sigma_{\rm tot}$, all four form factors must be included. Here we will only consider the results for $\sigma_{\rm tot}$. The maximum deviation of the nonstandard contribution $\Delta\sigma_{\rm tot}$ is about 11 pb ($\sim 50\%\ \sigma_{\rm tot}^{\rm SM}$), and is reached for $\lambda_Z=\lambda_\gamma=0.6$, $\Delta\chi_\gamma=-0.84$, and $\Delta\chi_Z=-0.57$.

By fixing two of the parameters (e.g., λ_Z,λ_γ), minimizing the deviation from the standard-model $\Delta\sigma_{\rm tot}$ with respect to the remainder free parameter (let us say $\Delta\chi_Z$), and assuming certain agreement (e.g., 50%) with the standard-model predictions, we would be able to exclude some regions in the two-dimensional parametric space ($\lambda_Z-\lambda_\gamma$). From $\Delta\sigma_{\rm tot}$, and with this procedure, we can set the bounds

$$-0.35\leq\lambda_\gamma\leq 0.35,\quad -0.35\leq\lambda_Z\leq 0.35\ , \tag{6.3}$$

for a 5% agreement.

In $\sigma_{\rm tot}$, taking both λ's to be equal (and assuming again a 50% agreement), we can get the allowed region for λ_γ ($=\lambda_Z$) and $\Delta\chi_Z$ ($\Delta\chi_\gamma$) showed in Fig. 5 (Fig. 6). As can be seen there, the results for λ's agree with (6.3). Figures 7 and 8 show the results for a e^+e^- machine of $\sqrt{S}=400$ GeV, where a 10% agreement with the standard model (Fig. 9, $\sigma_{\rm tot}^{\rm SM}$) has been assumed.

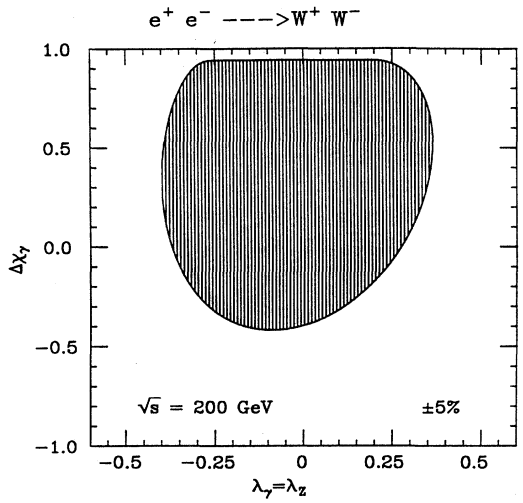

FIG. 6. The same as Fig. 5, but for $\Delta\chi_\gamma$ and λ_γ ($=\lambda_Z$).

Summarizing the previous results, assuming a 5% agreement with the standard model, experiments at LEP II would obtain the following bounds on the magnitude of the parameters.

(i) From σ_{LL},

$$-0.05\leq\Delta\chi_\gamma\leq 0.19,\quad -0.08\leq\Delta\chi_Z\leq 0.0\ , \tag{6.4}$$

or

$$0.61\leq\Delta\chi_\gamma\leq 0.80,\quad -0.19\leq\Delta\chi_Z\leq -0.09\ , \tag{6.5}$$

for the two ranges of Fig. 3.

(ii) From σ_{TT}

$$-0.30\leq\lambda_Z\leq 0.30,\quad -0.30\leq\lambda_\gamma\leq 0.30\ . \tag{6.6}$$

(iii) From $\sigma_{\rm tot}$

$$-0.35\leq\lambda_\gamma\leq 0.35,\quad -0.35\leq\lambda_Z\leq 0.35\ ,$$
$$-0.42\leq\Delta\chi_\gamma\leq 0.94,\quad -0.58\leq\Delta\chi_Z\leq 0\ . \tag{6.7}$$

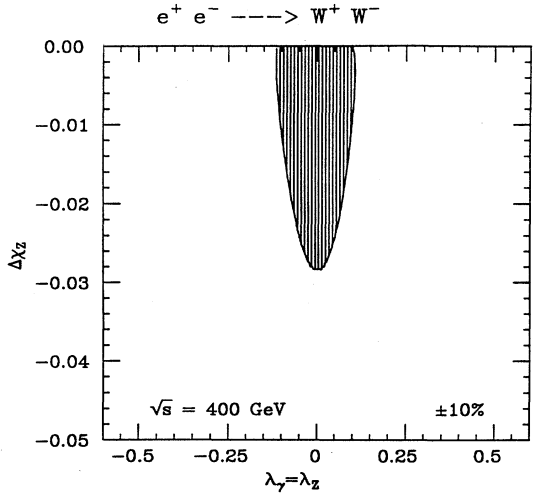

FIG. 7. The same as Fig. 4, but for an ILC machine ($e^+e^-\rightarrow W^+W^-$, $\sqrt{S}=400$ GeV) and 10% accuracy.

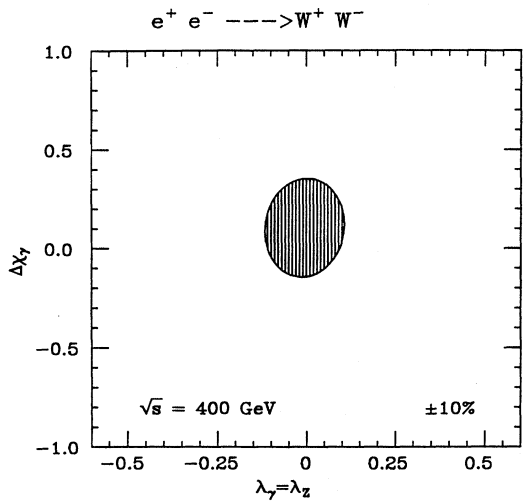

FIG. 8. The same as Fig. 5, but for an ILC machine ($e^+e^- \to W^+W^-$, $\sqrt{S}=400$ GeV) and 10% accuracy.

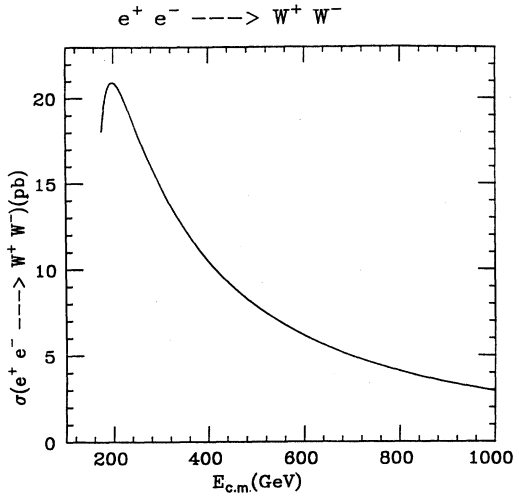

FIG. 9. Standard total cross section for $e^+e^- \to W^+W^-$ as a function of the c.m. energy.

Decreasing the accuracy in the measurements of the total cross section to 10%, the above bounds would become

(i) σ_{LL}

$$-0.14 \le \Delta\chi_\gamma \le 0.87, \quad -0.24 \le \Delta\chi_Z \le 0.0 \ . \tag{6.8}$$

(ii) σ_{TT}

$$-0.40 \le \lambda_Z \le 0.40, \quad -0.40 \le \lambda_\gamma \le 0.40 \ . \tag{6.9}$$

(iii) σ_{tot}

$$\begin{aligned} &-0.52 \le \lambda_\gamma \le 0.50, \quad -0.52 \le \lambda_Z \le 0.50 \ , \\ &-0.54 \le \Delta\chi_\gamma \le 0.94, \quad -0.77 \le \Delta\chi_Z \le 0.0 \ . \end{aligned} \tag{6.10}$$

A summary of the results for e^+e^- collider is given in Table I. Detailed explanation of bounds from ILC can be found in Appendix B.

It should be emphasized that the results of this section and the remainder of the paper only use tree-level diagrams and do not depend on the analysis of the low-energy data, except through using the results of Figs. 1 and 2 and the unitarity limits on λ_j to simplify the analysis (as explained in Sec. V).

A weakness of e^+e^- colliders compared with the hadron colliders is that all four parameters are involved, so less strong constraints can be obtained on any of them. If σ_{TT} and σ_{LL} could be measured, bounds on $(\lambda_Z,\lambda_\gamma)$ and $(\Delta\chi_Z,\Delta\chi_\gamma)$, separately, could be given. At the hadron colliders, sensitivity to only two parameters [$(\lambda_\gamma,\Delta\chi_\gamma)$ and $(\lambda_Z,\Delta\chi_Z)$, separately] per experiment is actually obtained because the WWZ and $WW\gamma$ vertices occur in different processes. Also, the WWZ and $WW\gamma$ vertices occur in diagrams suppressed by a neutral-current vertex for e^+e^-, while the diagrams of interest are more dominant for the hadron collider.

As we described before, when studying the sensitivity of the observables of e^+e^- to one of the couplings, no restrictions on the value of the other anomalous parameters has been made (aside from constraints and relations coming from low-energy data). For our analysis, we have assumed that only cross sections are measured. This gives

TABLE I. Bounds that will be obtained on the four nonstandard couplings λ_Z, λ_γ, $\Delta\chi_Z$, and $\Delta\chi_\gamma$, from LEP II, ILC, Tevatron, LHC, and SSC. Bounds from LEP II and ILC also assume low-energy and unitarity constraints. For hadron colliders (upgraded Tevatron, LHC, and SSC) we only assumed that the parameters have to be in the range of values allowed by low-energy data and unitarity. The propagation of the errors in the bounds coming from low-energy data have not been evaluated and the errors in the parameters are not given in the table. As a rough approximation, we think that the error for the upper bound (0.00) of $\Delta\chi_Z$ can be evaluated, from Fig. 1, as ± 0.04.

	LEP II 10% $\sqrt{s}=200$ GeV		ILC 10% $\sqrt{s}=400$ GeV	Tevatron 25% $\sqrt{s}=2$ TeV	LHC 25% $\sqrt{s}=17$ TeV	SSC 25% $\sqrt{s}=40$ TeV
	σ_{tot}	σ_{TT},σ_{LL}	$\int L\,dt=5\times10^3$ pb^{-1}	$\int L\,dt=10^3$ pb^{-1}	$\int L\,dt=10^4$ pb^{-1}	$\int L\,dt=10^4$ pb^{-1}
$\Delta\chi_Z$	−0.77–0.00	−0.24–0.00	−0.08–0.00	−0.08–0.00	−0.20–0.00	−0.15–0.00
λ_Z	−0.50–0.50	−0.40–0.40	−0.11–0.10	−0.36–0.30	−0.03–0.03	−0.02–0.02
$\Delta\chi_\gamma$	−0.54–0.94	−0.14–0.87	−0.15–0.35	−0.50–0.80	−0.20–0.20	−0.10–0.10
λ_γ	−0.50–0.50	−0.40–0.40	−0.11–0.10	−0.18–0.24	−0.02–0.02	−0.01–0.01

us a comparative idea of how well each collider (LEP II, ILC, Tevatron, LHC, and SSC) can constrain the anomalous couplings. The bounds will probably improve if differential cross sections are considered. For λ's and $\Delta\chi$'s, the bounds we got from LEP II [Eqs. (6.8)–(6.10), for a 10% accuracy], are approximately 5 times larger (4 times, if cross section for transverse W's is measured) and approximately 8 times larger (2 times, if cross section for longitudinal W's is considered), respectively , than those obtained by measuring the angular distribution of the produced W's (Ref. 10). Results similar to ours can be obtained by using polarized $e^{\pm}$ beams.[11] On the other hand, in both cases, the authors of Ref. 10 and 11 checked the sensitivity of the observables to one of the nonstandard parameters assuming values for the other anomalous couplings that are involved. We have avoided such assumptions. Notice that the cross sections are in general polynomials in the couplings, so there might be cancellations among the parameters, that could lead to bounds (when setting constraints on one of them) looser than those extracted by assuming some fixed values for the rest of the nongauge couplings.

VII. WZ AND $W\gamma$ PRODUCTION AT HADRON COLLIDERS

In this section we discuss what kind of bounds on the four form factors, $\Delta\chi_\gamma$, $\Delta\chi_Z$, λ_γ, and λ_Z, could be extracted from future experiments on $WZ\,(W\gamma)$ production at hadron colliders: (an upgraded) Tevatron, the LHC, and the SSC.

In this case, because there are only two free couplings $(\Delta\chi_V,\lambda_V)$ involved in each process, the analysis is more straightforward. We use the bounds on the magnitude of the parameters (listed in Sec. V) that we obtained from both the low-energy data and unitarity requirements. Notice that no relation between $\Delta\chi_V$ and λ_V (e.g., $\Delta\chi_\gamma$ and λ_γ, for $W\gamma$ production) will be imposed. The following discussion applies for the three colliders named above, Tevatron, LHC, and SSC, but for brevity the description of the procedure is given only for the SSC. The results for the three machines are given in Table I. In this section we assume an integrated luminosity of 10^4 pb^{-1} for SSC and LHC, and 10^3 pb^{-1} for an upgraded Tevatron; at a Tevatron collider of much lower luminosity useful limits are not obtained, though at 10^2 pb^{-1} some information is gained. To draw these conclusions we have assumed that reliable results can only be obtained from leptonic modes of W,Z; if hadronic modes can be used then correspondingly less luminosity is needed.

A. WZ Production

To extract the constraints on the two form factors $\Delta\chi_Z$ and λ_Z we adopt the following procedure.

Because the nonstandard contributions grow with the WZ invariant mass (M_{WZ}), the strongest constraints come from the behavior of the differential cross section $(d\sigma/dM_{WZ})$ as a function of M_{WZ} and $\Delta\chi_Z$ or λ_Z. For fixed M_{WZ} and λ_Z ($\Delta\chi_Z$) one can find the minimum deviation of $d\sigma/dM_{WZ}$ ($\equiv d\sigma^{\rm SM+NS}/dM_{WZ}$) from the standard-model prediction by minimizing $d\sigma^{\rm NS}/dM_{WZ}$ with respect to $\Delta\chi_Z(\lambda_Z)$. If the minimum deviation, at fixed M_{WZ}, exceeds a certain percentage (we take 25%) of the standard contribution $d\sigma^{\rm SM}/dM_{WZ}$, the $\lambda_Z(\Delta\chi_Z)$ is assumed to be excluded by the measurement. This ensures that, if agreement with the standard model is found, the value of a given parameter can never be bigger than the one set by the procedure described above, whatever the values of the other parameters. Nevertheless, because constraints found by this method for one of the couplings have not been used as input to constrain the other parameter, bounds might be looser than the ones one can get from a fit to real data. They are certainly looser than what some other authors have quoted by fixing some parameters by assumption.

In order to eliminate backgrounds at hadron colliders, we require both the W and Z to decay leptonically

$$Z\to e^+e^-,\mu^+\mu^-,\quad W^\pm\to e^\pm\nu,\mu^\pm\nu\ .$$

The branching ratios are

$$B(W^+\to e^+\nu)\simeq\tfrac{1}{12},\quad B(Z\to e^+e^-)\simeq 0.03\ . \qquad (7.1)$$

To identify the signal, one has to be able to reconstruct the momentum of the missing neutrino from W decay. Since there are two solutions for the longitudinal momentum (P_z^ν) of the missing neutrino, one has to fix a prescription to choose the one which will most likely give the correct distribution of the invariant mass of WZ. We tried two possible prescriptions: the dashed line in Figs. 10 and 11 is obtained by choosing the solution which has the smaller absolute value of P_z^ν; the dotted line is for the one which gives the smaller M_{WZ}. The solid line histogram in Fig. 10(11) is the theoretical prediction of the standard model for the SSC (upgraded Tevatron). These results are obtained using a parton level Monte Carlo program. From the good agreement shown in Figs. 10 and 11 of either method of choosing P_z^ν and the actual re-

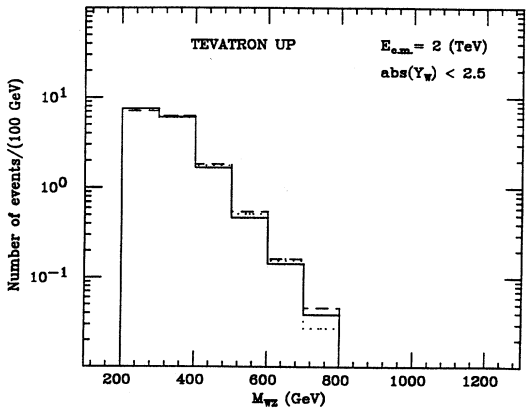

FIG. 10. Reconstruction of the shape of the differential cross section $d\sigma/dM_{WZ}$ for the pure leptonical decay mode at Tevatron. The dashed line correspond to a smaller absolute value of P_z^ν. The dotted line is for the one which gives the small M_{WZ}. The solid line is the theoretical prediction.

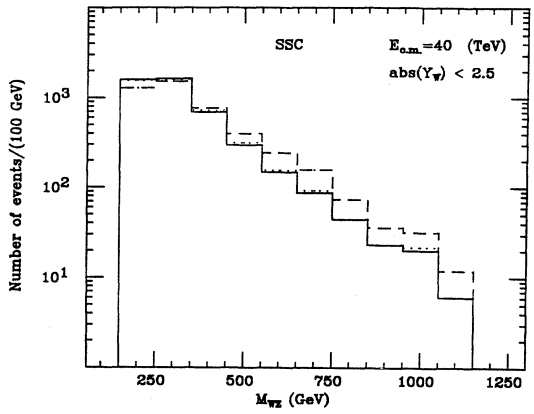

FIG. 11. The same as Fig. 10, but for the SSC.

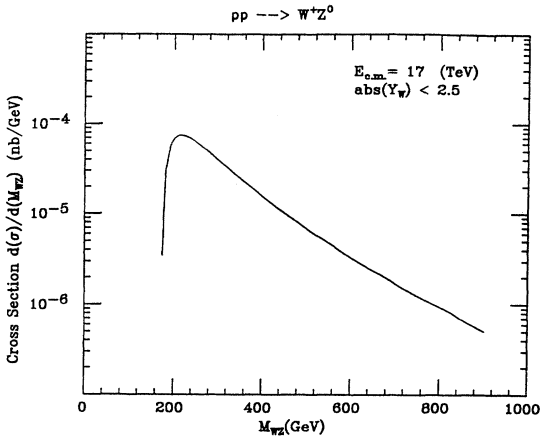

FIG. 13. The same as Fig. 12, but for LHC.

sult, we conclude that it is indeed possible to reconstruct the shape of the differential cross section $d\sigma/dM_{WZ}$ for the pure leptonical decay mode.

The differential cross sections $d\sigma^{\mathrm{SM}}/dM_{WZ}$ are shown in Figs. 12–14 (for Tevatron, LHC, and SSC, respectively) where a rapidity cut $|Y_W|<2.5$ has been imposed. From these figures one can see that, picking large invariant masses (which are more sensitive to anomalous couplings) has the disadvantages of reducing considerably the number of events. Our criterion, to obtain constraints on the couplings, will be to apply the procedure of minimum deviation (described in the previous paragraph) at the invariant mass that gives us at least 25 events in a 100-GeV bin. However, for the Tevatron, due to the small number of events, we require at least a three-standard-deviation effect to say that new physics is showing up; this leads to the result that no rigorous improvement in the bound of $\Delta\chi_Z$ can be obtained from Tevatron for 10^3 pb^{-1}.

However, since several parameters are involved, we want to emphasize that one can proceed in several ways.

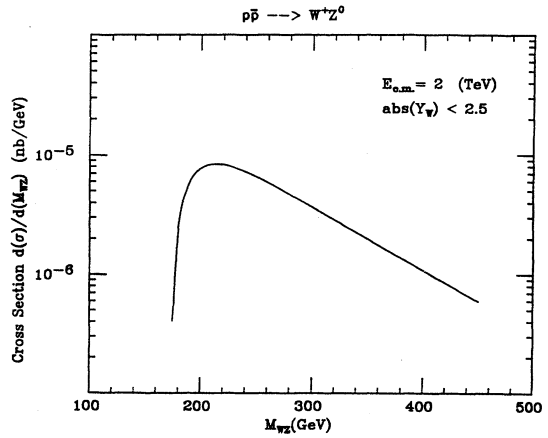

FIG. 12. Differential standard-model cross section for WZ production at the Tevatron as a function of the invariant mass M_{WZ}; decay branching ratios are not included.

We have given excluded ranges for parameters such that they are excluded for *any* values of other parameters. On the other hand, it can easily happen that a larger range of one parameter is excluded for *some* values of other parameters. Thus as soon as any experiment reaches the standard-model cross section, it begins to get useful restrictions, even if it cannot absolutely reduce the allowed ranges. Rather than compute all cases before there is data, we have only done the analysis one way. One example is that for the Tevatron, with an integrated luminosity of 10^2 pb^{-1}, the number of events expected from the standard model is very small (~ 2, in the range $200 \le M_{WZ} \le 400$), so little improvement on the bounds from low-energy data can be made, using the procedure of minimum deviation. However, for values of the couplings that give the maximum allowed deviation from the standard model, the number of events could be ~ 10, for the same range, so some improvement is achieved with such an integrated luminosity. This agrees with the result of Ref. 5, provided that only leptonic decays of the $W^{\pm}$ are considered. Once there is specific data for the Tevatron, improved bound are likely to result with close to 10^2 pb^{-1} of integrated luminosity.

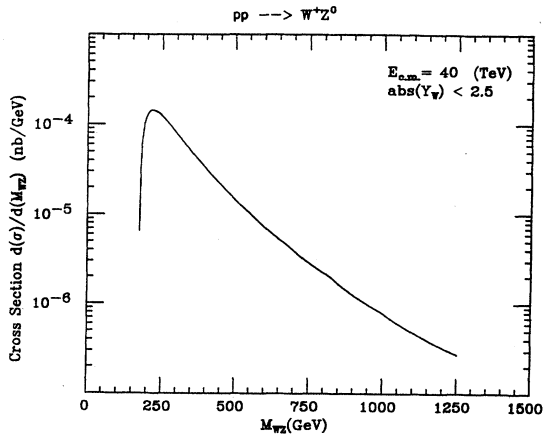

FIG. 14. The same as Fig. 12, but for the SSC.

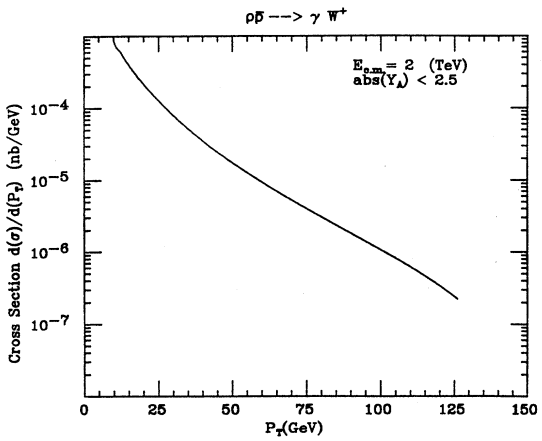

FIG. 15. Differntial standard model cross section for W_γ production at the Tevatron as a function of the transverse momentum of the photon P_T^γ; no branching ratio factor for W decay is included.

For the SSC, using the branching ratios for leptonic decays (7.1), we found that ~ 30 events can be expected in the range 850 GeV $\leq M_{WZ} \leq 950$ GeV, so one can extract the bounds on λ_Z and $\Delta\chi_Z$ shown in Table I. The same procedure was applied to LHC. The results are collected in Table I. There we can see that bounds for LHC and SSC are of the same order (smaller by a factor of 1–4) as the ones given in Ref. 4; but, on the other hand, we have not assumed any structure for the couplings.

B. $W\gamma$ production

The differential cross section $d\sigma^{\rm SM}/dP_T^\gamma$ are give in Figs. 15–17 (for Tevatron, LHC, and SSC, respectively), where P_T^γ is the transverse momentum of the photon, and a rapidity cut $|Y_\gamma| < 2.5$ has been imposed (see also Ref. 38). In this process the two form factors involved are λ_γ and $\Delta\chi_\gamma$. Following exactly the same analysis procedure given in Sec. VII A one can achieve the bounds on λ_γ and $\Delta\chi_\gamma$ presented in Table I. As for WZ production, the results for LHC and SSC are of the same order (smaller by a factor of 1–4) as those obtained in Ref. 23 where form factors with a certain structure were used. For the Tevatron, our bounds on λ_γ are a factor 2 better than those of Ref. 6, when an upgraded Tevatron with 10^3 pb^{-1} integrated luminosity is assumed. We have assumed that only leptonic decays of the W are used, $W \to e\nu$ or $\mu\nu$; if other modes can be used tighter bounds can be obtained.

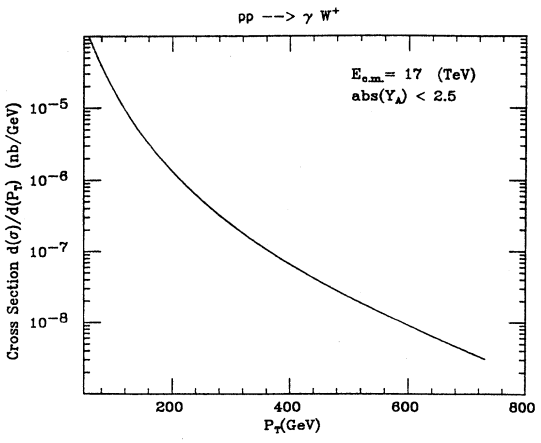

FIG. 16. The same as Fig. 15, but for the LHC.

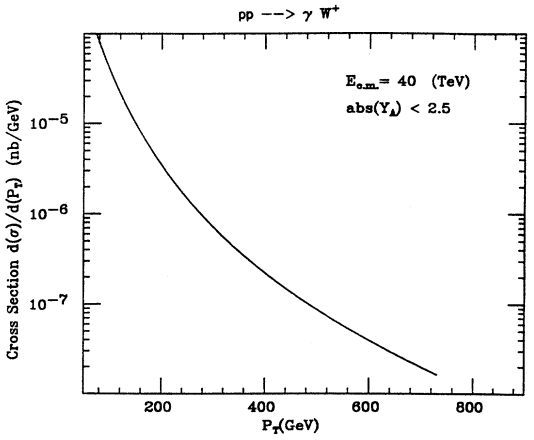

FIG. 17. The same as Fig. 15, but for the SSC.

VIII. DISCUSSION

In examining the implications of the low-energy data, we have adopted a regularization scheme to perform the required loop calculations so that the integration is well defined and not dependent on the way one does it; this procedure is Lorentz invariant, unlike the momentum cutoff scheme.

The results we have presented have to be seen as the loosest bounds each collider can set. The criterion used to fix the bounds on each anomalous coupling has led to some constraints looser than some of those found in the literature because we have not made any assumption (apart from those coming from low-energy data and unitarity) about the values of the other couplings that are involved. In this sense, our procedure assures us that for a value of one of the nonstandard couplings outside the allowed region, the measured cross section will always be bigger than the predicted standard-model value, no matter which values the rest of the anomalous couplings take (provided they are in the range allowed by low-energy data and unitarity). We have, then, excluded the possibility that a "conspiracy" between parameters can spoil the obtained bounds. Because we deal with more than one variable, this possibility is not excluded if one sets bounds on one of the parameters assuming the rest of them are zero (see, for example, Fig, 3; the region far from $\eta = 0$ can never be found if some couplings are set to zero). In a sense, we have given bounds which are or will be certainly satisfied, while most earlier authors have given examples of bounds that might be achieved if particular assumptions hold.

As we mentioned, in most of the cases some particular

combination of values for the couplings can give a big deviation of the measured cross section from the standard-model value. Once the cross section is measured, its value will probably imply tighter bounds, because restrictions on one of the parameters lead automatically to restrictions on the allowed values for the rest of the involved couplings. These correlations have not been taken into account in our calculations, so that some regions of allowed values for the parameters can actually be incompatible once the measurement is done; nevertheless we think that the analysis gives a good idea of how well different colliders can restrict the anomalous couplings.

The result of Ref. 14 is a special case of our Fig. 1 provided $\Delta\chi_\gamma=0$, apart from a factor of 3 due to the regularization procedure of the ultraviolet-divergent integrals.

Much better bounds than those presented in this work, for low-energy data and unitarity, can be found in Ref. 22 where a different Lagrangian, based on SU(2) global symmetry broken by electromagnetism,[31,7,9] is used. There unitarity limits were given in the absence of scalar contributions, and the one-loop corrections to M_W, M_Z, and ρ_M are performed without the redefinition (3.4) of the standard parameters, so terms of the form $\Lambda^4\delta$ appear. As we already mentioned in the analysis of the low-energy data (3), in our procedure we did not find this kind of extremely constraining conditions; they are an artifact of the regularization procedure.

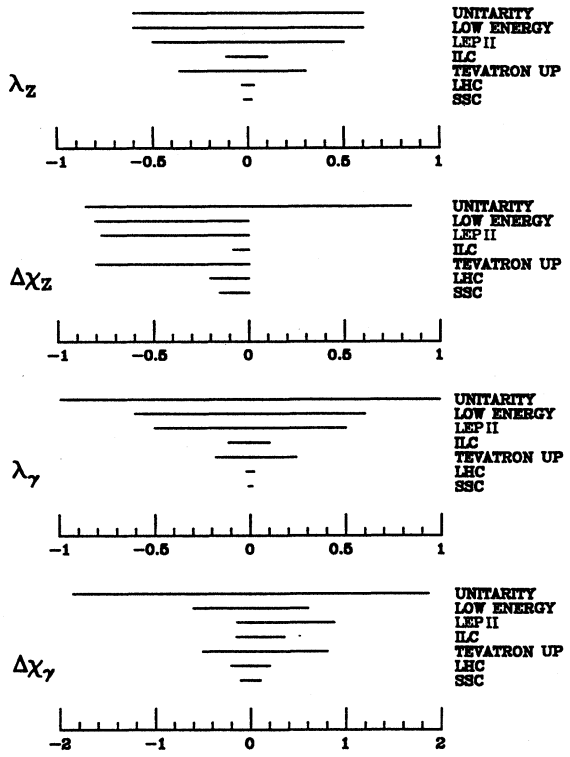

FIG. 18. Summary of bounds. Low-energy bounds for λ_Z and λ_γ use results also coming from unitarity. Bounds from LEP II and ILC also assume low-energy constraints (see Appendix B for a detailed discussion about bounds extracted from ILC). Hadron colliders (upgraded Tevatron, LHC, and SSC) assume the range of values for the nonstandard couplings are those given by low-energy data, but no relation among couplings is used.

IX. CONCLUSIONS

We have first studied the constraints that low-energy data can impose on the four C- and P-conserving anomalous couplings (λ_Z, λ_γ, $\Delta\chi_Z$, and $\Delta\chi_\gamma$). The results are somewhat improved compared with the ones coming from unitarity. Because of the loose bounds obtained from the low-energy existing data, we have examined how much those bounds can be restricted at future high-energy machines. The process $e^+e^-\to W^+W^-$ for e^+e^- colliders (LEP II and ILC), and WZ and $W\gamma$ production, for hadron colliders (Tevatron, LHC, and SSC), have been considered. For LEP II some of the relations obtained in low-energy experiments have been used to reduce the number of anomalous couplings involved. No relation among the couplings has been assumed for hadron collider experiments. We give the results for high-energy colliders in Table I. It shows the comparison for how well various facilities can do at restricting the four parameters that measure deviations from the WWZ and $WW\gamma$ vertices. The first column shows what can be achieved at LEP II, if an absolute measurement of $\sigma_{\rm tot}$ can be made to 10% accuracy. The second column is the analogous result if 10% accuracy can be achieved for σ_{LL} and σ_{TT} separately; that is very difficult since σ_{LL} is only a few percent of $\sigma_{\rm tot}$. In the third column we present the results for the ILC (400 GeV e^+e^- collider) for a 10% accuracy in $\sigma_{\rm tot}$. The Tevatron column show the analogous results for a 25% measurement of the $\sigma_{\rm tot}$ for an upgraded Tevatron. Only leptonic modes are used to reconstruct the ZW final state. The LHC and SSC column shows the numbers for the standard 17 TeV, 10^4 pb^{-1} and 40 TeV, 10^4 pb^{-1}, respectively, hadron colliders. In all cases the numbers improve if differential cross sections are measured,[10] but the relative effectiveness of various colliders is not affected much. The bounds are tighter for the LHC, SSC, and the Tevatron because they are sensitive to the shape of $d\sigma/dM_{WZ}$; at the Tevatron events can be detected for $20\le M_{WZ}\le 400$ GeV, at LHC for $600\le M_{WZ}\le 800$ GeV, and at the SSC for $800\le M_{WZ}\le 1000$ GeV. Figures 9 and 12–17 show the reach in M_{WW}, M_{WZ}, or P_T^γ; note the large extra leverage gained at ILC or at an upgraded Tevatron. Figure 18 summarizes our results for present and future tests.

ACKNOWLEDGMENTS

One of us (J.V.) is indebted to Consejo Superior de Investigaciones Científicas for financial support and to University of Michigan for hospitality. C.-P.Y. also wishes to thank Professor R. Akhoury and Professor Y. P. Yao for very useful discussions. This research was supported in part by the U.S. Department of Energy.

APPENDIX A

1. Self-energies for gauge bosons

Self-energies for gauge bosons are as follows:

$$\Pi_\gamma(q^2)=\frac{g^2}{24\pi^2}\frac{\Lambda^2}{M_W^2}s_W^2q^2\left[\frac{1}{4}\Delta X_\gamma\frac{q^2}{M_W^2}-3\lambda_\gamma-\Delta X_\gamma\lambda_\gamma+\tfrac{1}{8}\Delta X_\gamma^2\left[\frac{q^2}{M_w^2}-4\right]+\tfrac{1}{10}\lambda_\gamma^2\left[\frac{q^2}{M_W^2}+10\right]\right]-\frac{g^2}{24\pi^2}\frac{\Lambda^4}{M_W^4}\frac{1}{4}s_W^2q^2\lambda_\gamma^2\ , \tag{A1}$$

$$\Pi_Z(q^2)=\Pi_\gamma(q^2)(s_W\to c_W,\Delta X_\gamma\to\Delta X_Z,\lambda_\gamma\to\lambda_Z)\ , \tag{A2}$$

$$\begin{aligned}\Pi_W(q^2)=\frac{g^2}{24\pi^2}\frac{\Lambda^2}{4M_W^2}\Big[&\Delta X_Z^2c_W^2[\tfrac{5}{4}q^2-\tfrac{3}{2}M_W^2(2+1/c_W^2)]\\&+\Delta\chi_Zc_W^2[\tfrac{9}{2}q^2-3M_W^2(1+1/c_W^2)]+\tfrac{2}{5}\lambda_Z^2c_W^2\frac{q^2}{M_W^2}[q^2+5M_W^2(1+1/c_W^2)]\\&-4\Delta X_Z\lambda_Zc_W^2q^2-12\lambda_Zc_W^2q^2+\Delta X_\gamma^2s_W^2(\tfrac{5}{4}q^2-3M_W^2)\\&+\Delta\chi_\gamma s_W^2(\tfrac{9}{2}q^2-3M_W^2)+\tfrac{2}{5}\lambda_\gamma^2s_W^2\frac{q^2}{M_W^2}(q^2+5M_W^2)-4\Delta X_\gamma\lambda_\gamma s_W^2q^2-12\lambda_\gamma s_W^2q^2\Big]\\&-\frac{g^2}{24\pi^2}\frac{\Lambda^4}{M_W^4}\frac{1}{4}q^2(\lambda_Z^2c_W^2+\lambda_\gamma^2s_W^2)\ ,\end{aligned} \tag{A3}$$

$$\begin{aligned}\Pi_{\gamma Z}(q^2)=\frac{g^2}{24\pi^2}\frac{\Lambda^2}{M_W^2}s_Wc_Wq^2\Big[&\frac{1}{8}\frac{q^2}{M_W^2}(\Delta X_\gamma+\Delta X_Z)-\tfrac{3}{2}(\lambda_Z+\lambda_\gamma)\\&-\tfrac{1}{2}(\Delta X_\gamma\lambda_Z+\Delta X_Z\lambda_\gamma)+\tfrac{1}{8}\Delta X_Z\Delta X_\gamma\left[\frac{q^2}{M_W^2}-4\right]+\tfrac{1}{10}\lambda_Z\lambda_\gamma\left[\frac{q^2}{M_W^2}+10\right]\Big]\\&-\frac{g^2}{24\pi^2}\frac{\Lambda^4}{M_W^4}\frac{1}{4}s_Wc_Wq^2\lambda_Z\lambda_\gamma\ .\end{aligned} \tag{A4}$$

2. Effective couplings for $e^+e^-\to\mu^+\mu^-$ scattering

Defining the amplitudes

$$T_{VV}\equiv-\frac{e^2}{q^2}\bar v(e)\gamma^\mu u(e)\bar u(\mu)\gamma_\mu v(\mu)(1+h_{VV}),\quad T_{AA}\equiv-\frac{e^2}{q^2}\bar v(e)\gamma^\mu\gamma_5u(e)\bar u(\mu)\gamma_\mu\gamma_5v(\mu)h_{AA}\ , \tag{A5}$$

the effective couplings are given by

$$h_{VV}=h_{VV}^{\rm SM}+\Delta h_{VV},\quad h_{AA}=h_{AA}^{\rm SM}+\Delta h_{AA}\ , \tag{A6}$$

where

$$h_{VV}^{\rm SM}=\frac{q^2}{q^2-M_Z^2}\frac{1}{16s_W^2c_W^2}v^2,\quad h_{AA}^{\rm SM}=\frac{q^2}{q^2-M_Z^2}\frac{1}{16s_W^2c_W^2}a^2,\quad v=-1+4s_W^2,\quad a=-1\ , \tag{A7}$$

and the nonstandard contributions can be written as

$$\begin{aligned}\Delta h_{VV}=&\frac{\Pi_\gamma(q^2)}{q^2}\bigg|_{q^2=0}-\frac{\Pi_\gamma(q^2)}{q^2}+2\frac{q^2}{M_W^2}\Gamma^\gamma\\&+h_{VV}^{\rm SM}\left[\frac{M_Z^2}{q^2-M_Z^2}\delta_1-\frac{\Pi_Z(q^2)}{q^2-M_Z^2}-\frac{q^2}{q^2-M_Z^2}\left[\delta_2+\delta_3-\frac{s_W^2}{c_W^2}\delta_3\right]\right.\\&\left.-\frac{8}{v}\left[4s_W^2\Gamma^\gamma+\frac{q^2}{M_W^2}c_W^2\Gamma^Z\right]+\frac{8}{v}s_Wc_W\left[\frac{\Pi_{\gamma Z}(q^2)}{q^2}-\frac{\Pi_{\gamma Z}(q^2)}{q^2}\bigg|_{q^2=0}\right]\right]\\\Delta h_{AA}=&h_{AA}^{\rm SM}\left[-\frac{\Pi_Z(q^2)}{q^2-M_Z^2}+\frac{M_Z^2}{q^2-M_Z^2}\delta_1-\frac{q^2}{q^2-M_Z^2}\left[\delta_2+\delta_3-\frac{s_W^2}{c_W^2}\delta_3\right]-\frac{8}{a}c_W^2\frac{q^2}{M_W^2}\Gamma^Z\right]\ ,\end{aligned} \tag{A8}$$

with

$$\Gamma^i=\frac{g^2}{32\pi}\frac{\Lambda^2}{M_W^2}\frac{1}{24}\Delta X_i,\quad i=\gamma,Z\ . \tag{A9}$$

APPENDIX B

In this Appendix we give an analysis of the bounds that can be extracted from the total cross section $e^+e^-\to W^+W^-$ at $\sqrt{S}=400$ GeV, assuming that a 10% agreement with the standard-model value is measured.

The nonstandard cross section (in pb) for the process, in terms of the anomalous couplings, can be written as

$$\Delta\sigma=a\Delta\chi_\gamma^2+b\Delta\chi_Z^2+a_1\Delta\chi_\gamma+b_1\Delta\chi_\gamma+c\Delta\chi_Z\Delta\chi_\gamma+d\ , \tag{B1}$$

where a_1, b_1, and d are function of λ_Z and λ_γ given by

$$\begin{aligned} a_1&=-(4.29+5.75\lambda_\gamma+0.829\lambda_Z)\ ,\\ b_1&=-(2.46+0.829\lambda_\gamma+8.41\lambda_Z)\ ,\\ d&=37.5\lambda_\gamma^2+54.8\lambda_Z^2+1.27\lambda_\gamma+0.542\lambda_Z+10.8\lambda_Z\lambda_\gamma, \end{aligned} \tag{B2}$$

and the coefficients, a, b, and c, are 20.2, 29.5, and 5.82, respectively.

Equation (B1) corresponds to an ellipse in the $\Delta\chi_\gamma$-$\Delta\chi_Z$ plane. If 10% agreement ($|\Delta\sigma|\le 1$ pb) with the standard-model prediction is imposed, then we have

$$-1\le a\Delta\chi_\gamma^2+b\Delta\chi_Z^2+a_1\Delta\chi_\gamma+b_1\Delta\chi_\gamma+c\Delta\chi_Z\Delta\chi_\gamma+d\le 1\ . \tag{B3}$$

It turns out that the previous equation has a real solution if

$$\frac{a_1'^2}{a'}+\frac{b_1'^2}{b'}-4(d-1)\ge 0\ , \tag{B4}$$

with a', b', a_1', and b_1' defined in terms of the coefficients of Eq. (B3), as

$$\begin{aligned} a'&=a\cos^2\theta+b\sin^2\theta+c\cos\theta\sin\theta\ ,\\ b'&=a\sin^2\theta+b\cos^2\theta-c\cos\theta\sin\theta\ ,\\ a_1'&=a_1\cos\theta+b_1\sin\theta\ ,\\ b_1'&=-a_1\sin\theta+b_1\cos\theta\ ,\\ \tan 2\theta&=\frac{c}{a-b}\ . \end{aligned} \tag{B5}$$

In our case, Eq. (B4) is another ellipse, in the λ_γ-λ_Z plane

$$\frac{(\lambda_\gamma'+0.008)^2}{(0.188)^2}+\frac{(\lambda_Z'+0.003)^2}{(0.150)^2}\le 1\ , \tag{B6}$$

where λ_γ' and λ_Z' are the rotated axes (16°) in the clockwise direction. Equation (B6) establishes constraints for λ_Z and λ_γ, independently of the values of $\Delta\chi_Z$ and $\Delta\chi_\gamma$; only the values enclosed by the ellipse (B6) satisfy Eq. (B4), therefore, only these values are compatible with the measurement. The region obtained can be further restricted once some values (or allowed regions) for $\Delta\chi_Z$ and $\Delta\chi_\gamma$ are fixed. From (B6) we can extract the bounds

$$-0.15\le\lambda_Z\le 0.15,\quad -0.19\le\lambda_\gamma\le 0.18\ . \tag{B7}$$

These values have to be taken as limits for the parameters in the sense that the box represented by the bounds (B7) is the smallest one that contains the ellipse (B6). Once one of the parameters is fixed the other one becomes more constrained than (B7). Also, for given values (or regions) of $\Delta\chi_Z$ and $\Delta\chi_\gamma$, the left-side inequality of Eq. (B3) can exclude some values of the ellipse (B6).

The same procedure described below can be applied to the expression for the cross section written in the form

$$\Delta\sigma=\tilde a\Delta\chi_\gamma^2+\tilde b\Delta\chi_Z^2+\tilde a_1\Delta\chi_\gamma+\tilde b_1\Delta\chi_\gamma+\tilde c\Delta\chi_Z\Delta\chi_\gamma+\tilde d\ , \tag{B8}$$

with

$$\begin{aligned} \tilde a_1&=1.27-5.75\Delta\chi_\gamma-0.829\Delta\chi_Z\ ,\\ \tilde b_1&=0.542-0.829\Delta\chi_\gamma-8.41\Delta\chi_Z\ ,\\ \tilde d&=20.2\Delta\chi_\gamma^2+29.5\Delta\chi_Z^2-4.29\Delta\chi_\gamma-2.46\Delta\chi_Z\\ &\quad+5.82\Delta\chi_\gamma\Delta\chi_Z\ ,\\ \tilde a&=3.75,\quad \tilde b=54.8,\quad \tilde c=10.8\ . \end{aligned} \tag{B9}$$

Now the condition (B4) will restrict the allowed values of the $\Delta\chi_\gamma$ and $\Delta\chi_Z$ couplings to those enclosed by the ellipse

$$\frac{(\Delta\chi_\gamma'+0.09)^2}{(0.26)^2}+\frac{(\Delta\chi_Z'+0.06)^2}{(0.20)^2}\le 1\ , \tag{B10}$$

Again, the maximum and minimum values of each coupling is bounded to be in the range

$$-0.18\le\Delta\chi_Z\le 0.24,\quad -0.15\le\Delta\chi_\gamma\le 0.35\ . \tag{B11}$$

Notice that the bounds given by this method are independent of any other source of constraints for the nonstandard couplings. They have been obtained from the condition that the measured cross section has to agree with the standard-model prediction within a 10% accuracy.

If now, in addition, we impose the constraints by unitarity and low-energy data (for $\Lambda=1$ TeV), we see that no improvement for λ_Z and λ_γ is achieved. For $\Delta\chi_Z$ and $\Delta\chi_\gamma$, low-energy constraints and Eq. (B10) reduce the allowed values of the parameters to those enclosed by both the ellipse (B10) and the region between dashed lines in Fig. 1. From there, the maximum and minimum values that $\Delta\chi_Z$ and $\Delta\chi_\gamma$ may reach are

$$-0.08\le\Delta\chi_Z\le 0.04,\quad -0.15\le\Delta\chi_\gamma\le 0.35\ . \tag{B12}$$

Notice the improvement in the bounds for $\Delta\chi_Z$ due to the small overlap between low-energy and collider data,

along the $\Delta\chi_Z$ axis. If one uses the average curve in Fig. 1 to relate $\Delta\chi_Z$ and $\Delta\chi_\gamma$ (in the same way that we did for LEP II) the results for $\Delta\chi_Z$ (Fig. 7) are of the order of magnitude of the uncertainties in Fig. 1. It is clear now that in this case the whole region of Fig. 1 has to be used, and that the method which leads to the bounds (B12) is appropriate for combining low-energy data and very-high-energy e^+e^- collider data.

*On leave of absence from Departament de Física Teòrica, Universidad de València, and IFIC, Universidad de València–CSIC, Burjassot-València, Spain.

†Present address: Argonne National Laboratory, Argonne, IL 60439.

[1]M. Chanowitz, in *Proceedings of the UCLA Workshop on Observable Standard Model Physics at the SSC,* edited by H.-U. Bengtsson, C. Buchanan, T. Gottschalk, and A. Soni (World Scientific, Singapore, 1986); G. L. Kane, C.-H. Chang, and S.-C. Lee, Phys. Rev. D **37**, 101 (1988).

[2]J. Cortés, K. Hagiwara, and F. Herzog, Nucl. Phys. **B278**, 26 (1986).

[3]U. Baur and D. Zeppenfeld, Nucl. Phys. **B308**, 127 (1988).

[4]D. Zeppenfeld and S. Willenbrock, Phys. Rev. D **37**, 1775 (1988).

[5]S.-C. Lee and Wang-Chang Su, Phys. Lett. B **212**, 113 (1988).

[6]S.-C. Lee and Wang-Chang Su, Phys. Rev. D **38**, 2305 (1988).

[7]M. Kuroda, J. Maalampi, K. H. Schwarzer, and D. Schildknecht, Nucl. Phys. **B284**, 271 (1987).

[8]*1988 Summer Study on High Energy Physics in the 1990's,* Snowmass Colorado, 1988, edited by S. Jensen (World Scientific, Singapore, 1989); V. Barger and T. Han, Phys. Lett. B **212**, 117 (1988).

[9]J. Maalampi, D. Schildknecht, and K. H. Schwarzer, Phys. Lett. **166B**, 361 (1986); M. Kuroda, F. M. Renard, and D. Schildknect, Phys. Lett. B **183**, 366 (1987); M. Kuroda, J. Maalampi, D. Schildknecht, and K.-H. Schwarzer, *ibid.* **190**, 217 (1987).

[10]K. Hagiwara, R. D. Peccei, D. Zeppenfeld, and K. Hikasa, Nucl. Phys. **B282**, 253 (1987).

[11]D. Zeppenfeld, Phys. Lett. B **183**, 380 (1987).

[12]F. Olness and Wu-Ki Tung, Phys. Lett. B **179**, 269 (1986); V. Barger, T. Han, and R. J. N. Phillips, *ibid.* **39**, 146 (1989); S.-C. Lee and Wang-Chang Su, Phys. Lett. B **205**, 569 (1988); Z. Phys. C **40**, 547 (1988); Phys. Lett. B **214**, 276 (1988).

[13]H. Neufeld, J. D. Stroughair, and D. Schildknecht, Phys. Lett. B **198**, 563 (1987).

[14]J. A. Grifols, S. Peris, and J. Solá, Phys. Lett. B **197**, 437 (1987).

[15]J. A. Grifols, S. Peris, and J. Solá, Int. J. Mod. Phys. A **3**, 225 (1988).

[16]M. Suzuki, Phys. Lett. **153B**, 289 (1985).

[17]W. J. Marciano and A. Queijeiro, Phys. Rev. D **33**, 3449 (1986); J. J. van der Bij, *ibid.* **35**, 1088 (1987).

[18]A. Grau and J. A. Grifols, Phys. Lett. **166B**, 233 (1986).

[19]F. Herzog, Phys. Lett. **148B**, 355 (1984).

[20]A. Grau and J. A. Grifols, Phys. Lett. **154B**, 283 (1985); J. C. Wallet, Phys. Rev. D **32**, 813 (1985).

[21]R. Alcorta, J. A. Grifols, and S. Peris, Mod. Phys. Lett. **A2**, 23 (1987); *ibid.* **A3**, 1371(E) (1988).

[22]Y. Nir, Phys. Lett. B **209**, 523 (1988), and references therein.

[23]Y. Baur and D. Zeppenfeld, Phys. Lett. B **201**, 383 (1988).

[24]C. Bilchak, M. Kuroda, and D. Schildknecht, Nucl. Phys. **B299**, 7 (1988).

[25]K. O. Mikaelian, M. A. Samuel, and D. Sahdev, Phys. Rev. Lett. **43**, 746 (1979); M. Hellmund and R. Ranft, Z. Phys. C **12**, 333 (1982); R. W. Robinet, Phys. Rev. D **28**, 1185 (1983).

[26]K. O. Mikaelian, Phys. Rev. D **17**, 750 (1978); R. W. Brown, D. Sahdev, and K. O. Mikaelian, *ibid.* **20**, 1164 (1979); C. L. Bilchak, R. W. Brown, and J. D. Stroughair, *ibid,* **29**, 375 (1984); J. D. Stroughair and C. L. Bilchak, Z. Phys. C **26**, 415 (1985).

[27]D. A. Dicus and K. Kallianpur, Phys. Rev. D **32**, 35 (1985).

[28]C. L. Bilchak and J. D. Stroughair, Phys. Rev. D **30**, 1881 (1984).

[29]Zhu Dongpei, Phys. Rev. D **22**, 2266 (1980); C. J. Goebel, F. Halzen, and J. P. Leveille, *ibid.* **23**, 2628 (1981); S. J. Brodsky and R. W. Brown, Phys. Rev. Lett. **49**, 966 (1982); R. Brown, K. L. Kowalski, and S. J. Brodsky, Phys. Rev. D **28**, 624 (1983); M. A. Samuel, *ibid.* **27**, 2724 (1983).

[30]K. J. F. Gaemers and G. J. Gounaris, Z. Phys. C **1**, 259 (1979); K. Hikasa, Phys. Lett. **128B**, 253 (1983).

[31]P. Q. Hung and J. J. Sakurai, Nucl. Phys. **B143**, 81 (1978); J. D. Bjorken, Phys. Rev. D **19**, 335 (1979).

[32]H. Aronson, Phys. Rev. **186**, 1434 (1969).

[33]M. Green and M. Veltman, Nucl. Phys. **B169**, 137 (1980); **B175**, 547 (1980); F. Antonelli, G. Corbo, M. Consoli, and O. Pellegrino, *ibid.* **B183**, 195 (1981).

[34]U. Amaldi *et al.*, Phys. Rev. D **36**, 1385 (1987).

[35]R. Cahn and F. Gilman, Phys. Rev. D **17**, 1313 (1978); E. Derman and W. Marciano, Ann. Phys. (N.Y.) **121**, 147 (1979).

[36]C. Y. Prescott *et al.*, Phys. Lett. **77B**, 347 (1978); **84**, 524 (1979).

[37]G. Barbiellini *et al.*, CERN Report No. 86-02, 1986 (unpublished).

[38]S. A. Kahn, T. J. Killian, M. J. Murtagh, and F. E. Paige, BNL Report No. 3/83 (unpublished).